Three dominant synoptic atmospheric circulation patterns influencing severe winter haze in eastern China

Shiyue Zhang[1], Gang Zeng[1]*, Tijian Wang[2], Xiaoye Yang[1], Vedaste Iyakaremye[3]

[1]Key Laboratory of Meteorological Disaster, Ministry of Education, Collaborative Innovation Center on Forecast and Evaluation of Meteorological Disasters (CIC-FEMD), Joint International Research Laboratory of Climate and Environment Change (ILCEC), Nanjing University of Information Science and Technology, Nanjing, China, 210044

[2]School of Atmospheric Sciences, Nanjing University, Nanjing, 210023, China

[3]Rwanda Meteorology Agency, Nyarugenge KN 96 St, Kigali, Rwanda

Correspondence to: Gang Zeng (zenggang@nuist.edu.cn)

Abstract. Previous studies indicated that, on synoptic scale, the severe haze in eastern China (EC) is affected by the atmospheric circulation variations. However, it is still unclear what are the dominant atmospheric circulation patterns influencing the severe winter haze conditions in EC and what are the differences between them. To systematically determine the dominant synoptic atmospheric circulation patterns of severe haze in different regions of EC, we use the Hierarchical Clustering Algorithm to classify the local geopotential height anomalies at 500-hPa over the stations with severe haze and obtained three dominant synoptic atmospheric circulation types based on observed $PM_{2.5}$ concentration and NCEP/NCAR reanalysis. Circulation Type1 is accompanied by significant north wind component anomalies over northern China and causes severe haze pollution over the Yangtze River valley. Although the local meteorological conditions are not conducive to haze formation and accumulation, the severe haze in Yangtze River valley is related to the pollution transportation caused by the north wind anomalies. During the haze days with circulation Type2, the joint affection of East Atlantic-West Russia teleconnection pattern and winter East Asia subtropical jet stimulate and maintain the anticyclonic anomalies over northeast Asia, which provides meteorological conditions conducive to the occurrence of severe haze over the whole EC. The circulation Type3 mainly caused severe haze events in northeast China through the establishment of blocking high over the Okhotsk Sea. The results provide a basis for establishing haze prediction and management policies applicable to different regions in EC.

1. Introduction

Severe haze could increase the risk of traffic accidents by reducing visibility and harm human health by causing respiratory diseases (Xie et al., 2014; Hu et al., 2015; Wang et al., 2016). Haze events in China are mainly caused by $PM_{2.5}$ (particulate with an aerodynamic diameter less than 2.5μm; Cai et al., 2017; Shen et al., 2018; Wang et al., 2021). Researches show that the distribution of haze days in China has the characteristics of uneven spatial distribution, with more in economically developed eastern region and less in economically underdeveloped region (Wu et al., 2013; Liu et al., 2015; Xu et al., 2015). With the rapid development of industrialization, urbanization and increase in anthropogenic emission, eastern China (EC) has experienced more severe haze events with long duration, large spatial scale, and serious harm in the past few decades (Monks et al., 2009; Qian et al., 2009; Wang et al., 2009). Since the beginning of the 21st century, the uneven spatial distribution of haze events in China have become more obvious (Sun et al., 2016), which has led to the increasing incidence rate and mortality related to respiratory diseases in Beijing-Tianjin-Hebei, the Yangtze River valley, and the Pearl River Delta (Tsaia et al., 2014; Ding et al., 2016; Fan et al., 2019). Although haze pollution control in China has been improved to some extent with the strict implementation of energy conservation and emission reduction policies after 2013 (Wang et al., 2021), it still affects various socio-economic sectors and human health.

In addition to human activities, meteorological conditions are also considered as one of the most important factors for determining regional air quality. Previous studies have indicated that, on the weather scale, the formation and maintenance of haze days in eastern China (HD_{EC}) are closely related to favorable weather conditions (Niu et al., 2010; Cai et al., 2017), including strong thermal inversion potential, high relative humidity, negative sea level pressure anomaly, and weak wind speed. Furthermore, the anticyclonic anomaly could lead to the sinking movement and weaker thermal inversion potential, which inhibit the vertical diffusion of pollutants and affect the air quality of the local or larger region (Wu et al., 2013; Xu et al., 2015). Many studies investigated the key circulation system affecting HD_{EC} from an interannual scale or intraseasonal scale and suggested that the weak East Asian Winter Monsoon (Li et al., 2015; Yin et al., 2015; Zhang et al., 2022), the positive phase of Arctic Oscillation (Wang et al., 2015; Yin et al., 2015) and the positive phase of East Atlantic-West Russia (EA/WR) teleconnection pattern (Yin et al., 2017) could result in more

haze days in China. On the synoptic scale, meteorological conditions could also significantly regulate HD_{EC}. The weak synoptic circulation with a high-pressure or continuous low-pressure system is beneficial for the accumulation of pollution, while the strong weather phenomena with a large pressure gradient encourage the diffusion of pollutants (Li et al., 2019; Cai et al., 2020). Furthermore, studies have shown that cold surges can dissipate and reduce local air pollutants by bringing dry and clean cold air (Wu et al., 2017; Leung et al., 2018; Zhang et al., 2021).

A recent study classified the daily winter circulation anomalies and suggested that there are two dominant climate drivers (i.e., EA/WR teleconnection pattern and Victoria mode of sea surface temperature anomalies) conducive to the severe haze occurrence in North China (Li et al., 2022). Existing studies have also investigated the synoptic circulation patterns conducive to haze pollution in different regions of China (Chang and Zhang, 2017; Li et al., 2019; Liu et al., 2019; Liao et al., 2020; Sun et al., 2020; Yang et al., 2021; Gong et al., 2022). Most of these studies produced the classification based on low-level circulation anomalies, while the upper-level circulation also play an important role in the generation and accumulation of haze (Wang et al., 2015; Yin and Wang, 2017; Zhong et al., 2019). In addition, due to the large spatial span in EC, if we assess the classification of synoptic circulation patterns in a fixed region, it may lead to different effects of the same classification pattern on different regions. Therefore, we classify the circulation anomalies with severe haze days of each station in EC respectively, and finally obtain the dominant synoptic atmospheric circulation pattern of each station. In general, the present study addresses the following scientific questions: (1) what are the synoptic atmospheric circulation patterns that dominate severe haze pollution in EC, (2) what are the differences in the action range of each circulation pattern, and what are their possible mechanisms. These issues are addressed using a modified classification algorithm (Hierarchical Clustering Algorithm) that is more suitable for studying the classification of synoptic patterns in a large spatial range.

The remaining sections of this paper are structured as follows: Data and definitions are introduced in section 2. Section 3 shows the dominant synoptic circulation patterns of severe HD_{EC}. In section 4, we compare different circulation types associated with severe HD_{EC}. Finally, the discussion and main conclusions are given in section 5.

2. Data and Methods

2.1 Data

In this study, the daily meteorological data and the observed $PM_{2.5}$ concentrations from 2014 to 2021 were used to analyze the dominant circulation patterns and their main causes of severe haze in winter in EC. The daily NCEP/NCAR reanalysis was obtained from https://psl.noaa.gov/, which includes sea level pressure (SLP), surface air temperature (SAT), the temperature in multiple pressure levels, geopotential height (GPH), three-dimensional wind, relative humidity (RH) at 1000-hPa, and vertical velocity (omega) at 850-hPa (Kalnay et al., 1996). The dataset has a horizontal resolution of 2.5°× 2.5°. In this study, we defined the thermal inversion potential (TIP) as the air temperature at 850-Pa minus SAT referring to Yin and Wang (2019). The Daily $PM_{2.5}$ concentrations for 935 meteorological stations in China (following Yin and Wang (2016) and Yin et al. (2021), the stations with missing data more than 5% of are dropped; the stations with data lost continuously for 3 days or more is also discarded) were obtained from China National Environmental Monitoring Centre (https://quotsoft.net/air/). The sporadic missing data (less than 3 days) were filled by cubic spline interpolation.

2.2 Definition of severe HD_{EC}

In this study, the severe HD_{EC} is defined when $PM_{2.5}$ concentration $\geqslant$150 μg m^{-3} (Cai et al., 2017; Zhong et al., 2019). We focused on the haze days in the cool season (November to February of the following year, abbreviated as NDJF), which accounts for more than 40% of the total haze days in China in a year (Sun et al., 2013; Wang et al., 2015). Figure 1 shows the climatology of haze days in China from 2014 to 2021 in NDJF. The severe haze days are mainly concentrated in the EC (east of 105°E and south of 54 °N), which is selected as the target area in the present study. Thus, a subset of 853 stations is selected.

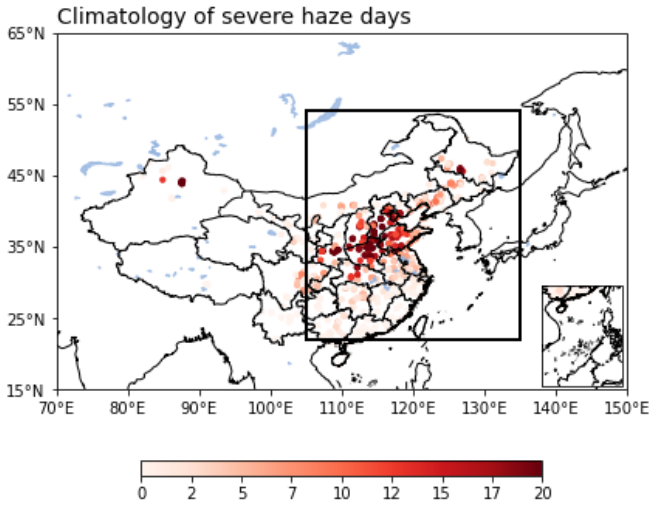

Figure 1. Spatial distribution of the annual averaged severe haze days (unit: day) in China from 2014 to 2021 in NDJF. The black box represents EC.

2.3 Definition of blocking index

In winter, the anticyclone anomaly over the Okhotsk Sea, usually related to atmospheric blocking, may lead to haze accumulation (Yun and Yoo 2019; Hwang et al., 2022). Thus, based on previous studies (Tibaldi et al., 1990; Fang and Lu, 2020), here we identify the blockings by northward gradients (GHGN) and southward gradients (GHGS) of Z_{500} at each grid point:

$$GHGN = \frac{z_{500}(\lambda,\phi+\Delta\phi)-z_{500}(\lambda,\phi)}{\Delta\phi} \quad (1)$$

$$GHGS = \frac{z_{500}(\lambda,\phi)-z_{500}(\lambda,\phi-\Delta\phi)}{\Delta\phi} \quad (2)$$

Where ϕ = 35°, 35.5° …, 75°N, λ = 70°, 70.5° …, 160°E and $\Delta\phi$ = 15°. A given longitude is defined as "blocked" at a particular time satisfies the following conditions:

$$GHGS > 0,\ GHGN < -10 \text{ m (deg lat)}^{-1}$$

Based on these conditions, we can identify whether any grid in the range of 35°N-70°N is blocked at any time.

2.4 Plumb's wave activity flux

Here we used the wave flux of Rossby to show the propagation of wave energy (Plumb, 1985). The two-dimensional Plumb's wave activity flux can be expressed by:

$$F_s = \frac{P}{P_0}\cos\varphi \times \begin{pmatrix} v'^2 - \frac{1}{2\Omega \sin 2\varphi}\frac{\partial(v'\phi')}{\partial\lambda} \\ -u'v' + \frac{1}{2\Omega \sin 2\varphi}\frac{\partial(u'\phi')}{\partial\lambda} \end{pmatrix} \quad (3)$$

In Eq. (3), F_s (unit: m^{-2} s^{-2}) denotes the horizontal stationary wave activity flux, P means the pressure; P_0 =1000-hPa, u' and v' are the zonal and meridional wind deviation, respectively. And the ϕ' is geopotential height. φ (λ) represents the latitude (longitude). a is the radius of Earth, and Ω means Earth's rotation rate.

2.5 Classification algorithm of synoptic atmospheric circulation

This paper uses the hierarchical clustering algorithm (HCA) to classify the severe HD_{EC} based on the associated circulations anomalies. Based on HCA (Rokach et al., 2005), we could create a clustering tree of data samples by calculating the Euclidean distance between different categories. The original data samples of different types are at the lowest level of the tree, and the root point of a cluster is at the top level of the tree.

Unlike Li et al. (2022), we only cluster the circulation anomalies of days with severe HD_{EC}, which can ensure that all classification samples lead to $PM_{2.5}$ at least one station in EC exceeds the standard of severe haze pollution and produce more accurate classification types. Secondly, the circulation samples selected are not in a fixed region, but the rectangular regions of the same size centered on each station with severe haze. Since the upper-level circulation represented by 500-hPa geopotential height anomalies play an important role in the generation and accumulation of haze (Wang et al., 2015; Yin and Wang, 2017; Zhong et al., 2019), the GPH anomalies at 500-hPa in a rectangular region of 30 degrees from east, west, north, and south with each station as the center on the day of severe HD_{EC} were taken as the samples to perform HCA. It means that our classification results focus on the local circulation anomalies accompanied by haze, which can help us more accurately understand the impact of different local circulation patterns on different stations. Specifically, this clustering scheme can ensure that each station is located in the center of the circulation pattern when severe haze occurs, and avoid the impact of circulation pattern movement. The final composite results of the same pattern can reflect the average statement of the current type of circulation anomaly, which is helpful to investigate its possible physical mechanism.

We use the silhouette coefficient to determine the optimal classification result (Rousseeuw, 1987). For any sample i, the silhouette coefficient $s(i)$ is defined as:

$$s(i) = \frac{b(i)-a(i)}{max\{a(i),b(i)\}} \quad (4)$$

$a(i)$ means the average distance from sample i to all other samples in the cluster it belongs to, and $b(i)$ means the lowest average distance from sample i to all samples in any other cluster. The silhouette coefficient of the clustering result is the average of the silhouette coefficients of all samples. The closer to 1, the better the classification results. Figure S1 shows the clustering tree and its associated silhouette coefficient of this study.

3. Dominant synoptic atmospheric circulation patterns of severe HD_{EC}

Figure 2a shows the composite anomalies of 500-hPa GPH during all severe HD_{EC} in 853 stations. Generally, the stations with severe haze are located in the southwestern parts of the anticyclonic anomaly center, which is consistent with previous studies (Zhong et al., 2019; Wang and Zhang, 2020). Then we performed the HCA as described in Section 2.5 and obtained three types of dominant local circulation anomalies associated with the severe HD_{EC} (Figure 2b, c, d). Circulation Type1 shows a wave-train structure of '+ - +', and the stations are located in the west of anticyclonic anomaly and the south of cyclonic anomaly. Circulation Type2 shows the circulation anomalies similar to Figure 2a. Finally, circulation Type3 denotes that the stations are located south of the anticyclonic anomaly, and the intensity and range of the anticyclonic anomaly are significantly stronger than the other two patterns. The differences between the types imply that severe HD_{EC} may be related to different causes.

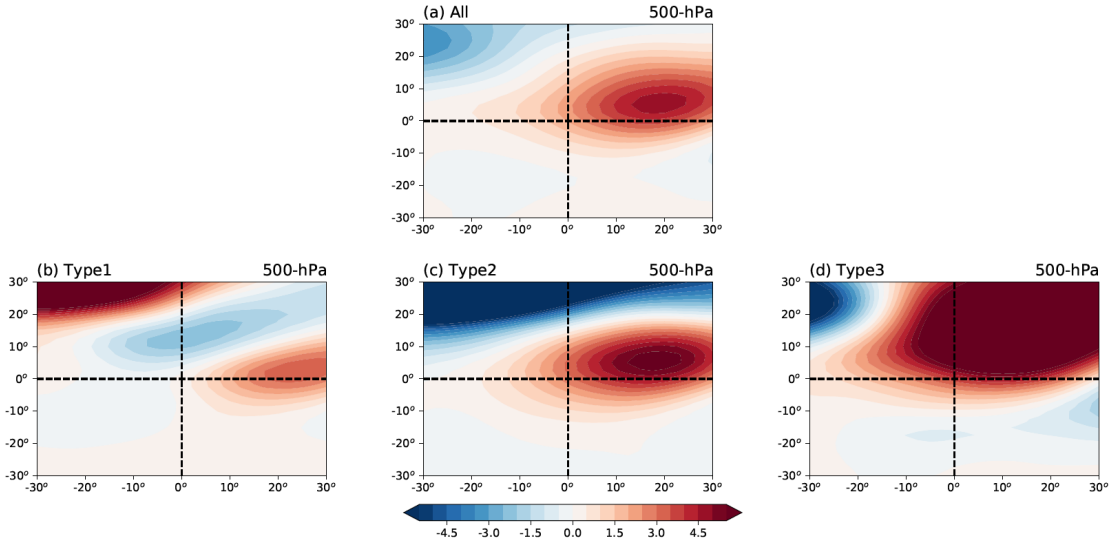

Figure 2. (a) Composite anomalies of GPH at 500-hPa (units: gpm) during all severe HD_{EC} in 853 stations. (0°, 0°) represents the location of stations. (b), (c), and (d) are same as (a) but for three sub-types.

For each station, when the probability of a certain circulation type is greater than the sum of the other two types, we define this type as the dominant type of the station. Figure 3 shows the leading circulation types of severe HD_{EC} for 853 stations and the weighted probability density distribution of three circulation types (the weight of each station is the probability of the corresponded dominant type occurring at the station). Stations dominated by the circulation Type1 are mainly distributed in the Yangtze River valley (YRV). The stations dominated by the circulation Type2 cover almost the whole EC, with two centers in South China (SC) and Beijing-Tianjin-Hebei region. The stations dominated by the circulation Type3 are mainly located in Northeast China (NEC). In general, the stations in the north of EC are accompanied by higher $PM_{2.5}$ concentration and more haze days (Figure S2). These results suggest significant differences in the circulation patterns of severe haze in different regions of EC.

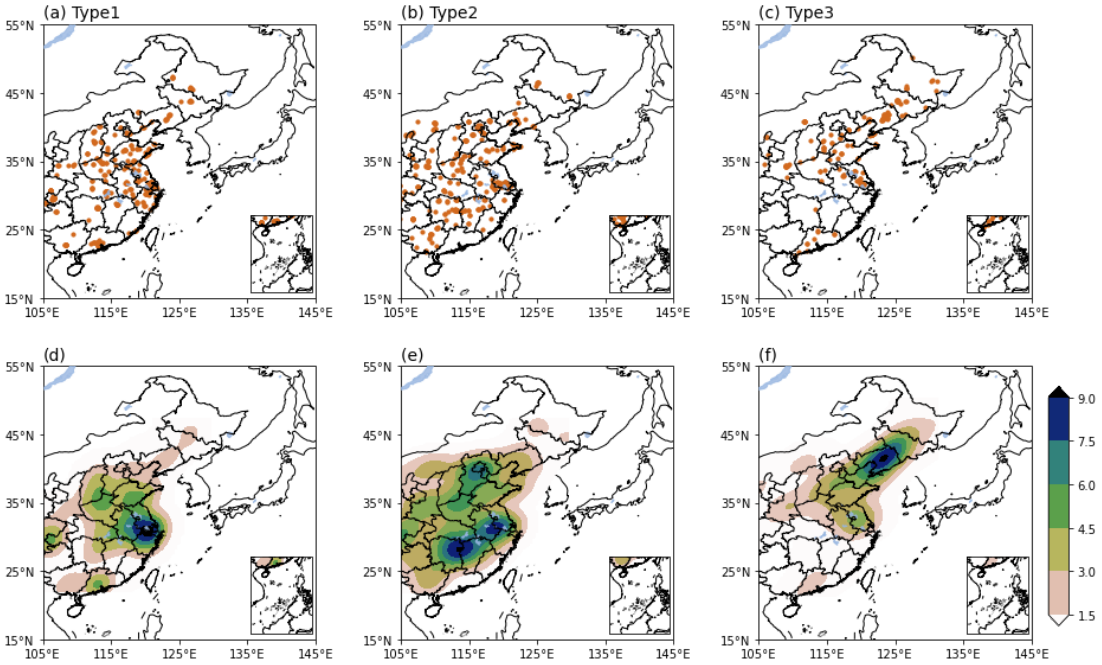

Figure 3. Distribution of stations dominated by (a) Type1, (b) Type2, and (c) Type3 synoptic circulation pattern. Weighted probability density distribution of stations dominated by (d) Type1, (e) Type2, and (f) Type3 synoptic circulation pattern.

4. Comparison of different circulation types associated with severe HD_{EC}

Figure 4a, b, and c show the composite anomalies of circulation Type1 at 500-hPa and 850-hPa. The circulation Type1 is associated with the upper troposphere's wave-train structure of "- + -". Unlike previous studies (Zhong et al., 2019; Wang and Zhang, 2020), there are no significant anticyclonic anomalies in the mid-troposphere over YRV, but with substantial north wind component in the lower troposphere over northern China. The TIP, sinking movement, and RH anomalies over the YRV are weak (Figure 4d, e, f). Therefore, it can be inferred that it is not the local circulation anomalies that promote the formation and accumulation of haze pollution, but the regional haze transportation caused by the north wind component anomalies that leads to the severe haze in the YRV.

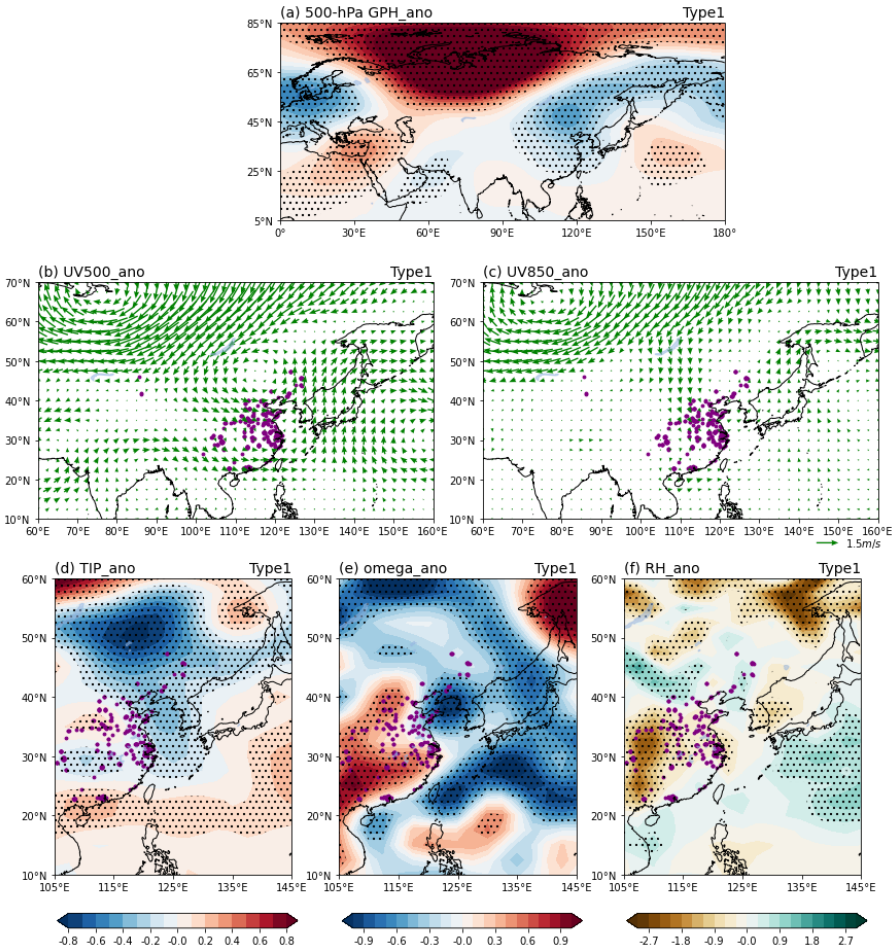

Figure 4. Composite anomalies of (a) GPH at 500-hPa (unit: gpm), horizontal wind (unit: m s^{-1}) at (b) 500-hPa and (c) 850-hPa, (d) TIP (unit: K), (e) omega (unit: 10^{-2} Pa s^{-1}), and (f) RH (unit: %) for circulation Type1. Dotted areas are statistically significant at the 95% confidence level. The purple dots represent the stations dominated by circulation Type1.

To further explore the relationship between Type1 severe HD_{EC} and north wind component anomalies, we present the evolution of $PM_{2.5}$ concentration variations ($PM_{2.5}$ concentration on Day_i minus that on Day_{i-1}) from -3 days to 2 days of Type1 severe HD_{EC} occur (Figure 5a, b, c, d, e) and the corresponding horizontal wind variations at 500-hPa (Figure 5 f, g, h, i, j). $PM_{2.5}$ concentration tends to increase at first and then dissipate showing an obvious transportation process from north to south. Accordingly, the horizontal wind changes from anticyclonic anomalies to cyclonic anomalies, with the south wind turning to the north wind. Here we average the $PM_{2.5}$ concentration variations in Figure 5a, b, c, d, e, and meridional wind variations in Figure 5f, g, h, i, j along latitudes (Figure 5k, l, m, n, o). The result shows that $PM_{2.5}$ concentration gradually increased from north EC to south

EC and began to decrease after severe HD_{EC} occurred. With the variation in $PM_{2.5}$ concentration, the south wind in the north EC gradually weakens and turns to the north wind when severe HD_{EC} occurs. With the dry and cold air from the north invading southward, the haze dissipates rapidly, and EC can maintain high air quality weather. Therefore, although circulation Type1 will lead to severe haze in YRV, its circulation anomalies do not match the conditions to maintain haze pollution.

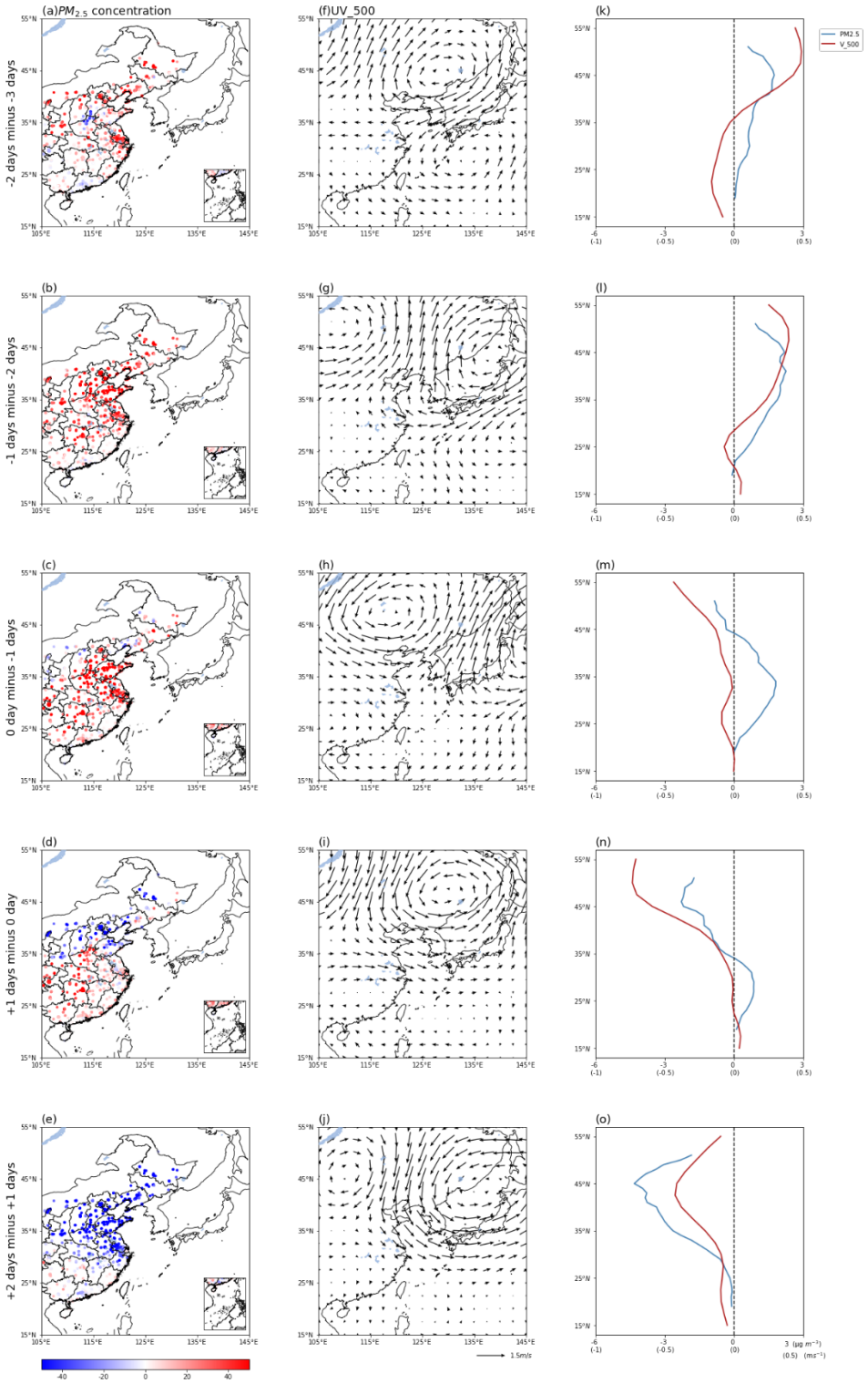

Figure 5. Composite anomalies of (a-e) the spatial distribution of $PM_{2.5}$ concentration (unit: μg m^{-3}) from -3 days to 2 days related to Type1 severe HD_{EC} occur and (f-j) the corresponding horizontal wind (unit: m s^{-1}) at 500-hPa. (k-o) shows the zonal averaged $PM_{2.5}$ concentration variations (unit: μg m^{-3}) and meridional wind variations (unit: m s^{-1}) in the range of 15-55°N, 105-135°E.

During the occurrence of circulation Type2, there was an anticyclonic anomaly with a quasi-barotropic structure over Northeast Asia, and the EC was located in the southwest of the anticyclone (Figure 6a, b, c). The significant positive TIP, sinking movement, and positive RH anomalies control the region over EC (Figure 6d, e, f). With the increase in TIP and the warm and humid air from the sea transports to the EC, the horizontal and vertical dispersion of pollutants was restrained, while higher surface RH exacerbated the formation of particulates. Such circulation anomalies are beneficial for the formation and maintenance of haze pollution.

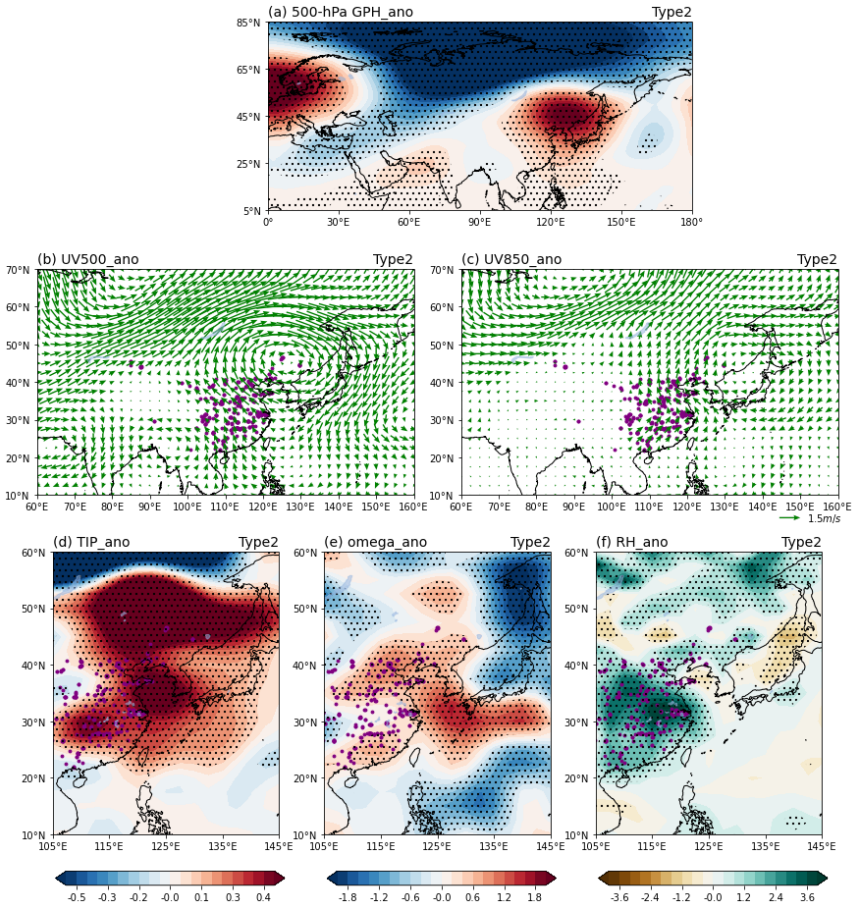

Figure 6. Composite anomalies of (a) GPH at 500-hPa (unit: gpm), horizontal wind (unit: m s^{-1}) at (b) 500-hPa and (c) 850-hPa, (d) TIP (unit: K), (e) omega (unit: 10^{-2} Pa s^{-1}), and (f) RH (unit: %) for circulation Type2. Dotted areas are statistically significant at the 95% confidence level.

Here we investigate the dynamic mechanism of the circulation Type2 by compositing the GPH and WAF anomalies in the upper troposphere. The circulation anomalies show two quasi-zonal wave trains over the mid-high latitudes. The one is characterized by a '-+-+' pattern of GPH anomalies from the south of Greenland across Siberia to Northeast China, with positive GPH anomalies in the second and fourth centers. Such anomalies are similar to the positive phase of EA/WR teleconnection, which can strengthen stable weather conditions over EC (Wu et al., 2016; Yin and Wang, 2016) by causing weak wind speed, higher RH, and strong TIP (Niu et al., 2010; Ding and Liu, 2014; Cai et al., 2017). Figure 7c shows the correlation coefficients between $PM_{2.5}$ concentration during the occurrence of circulation Type2 and the EA/WR index (The EA/WR index was computed by the NOAA climate prediction center according to the rotated principal component analysis used by Barnston and Livezey (1987)). The results show significant positive correlations between the two in north EC and weak negative correlations in south EC. However, the circulation Type2 caused the severe HD_{EC} for almost the whole EC, which is not completely consistent with the results of Figure 7c. Therefore, we speculate that the other wave-train may lead to haze pollution in south EC.

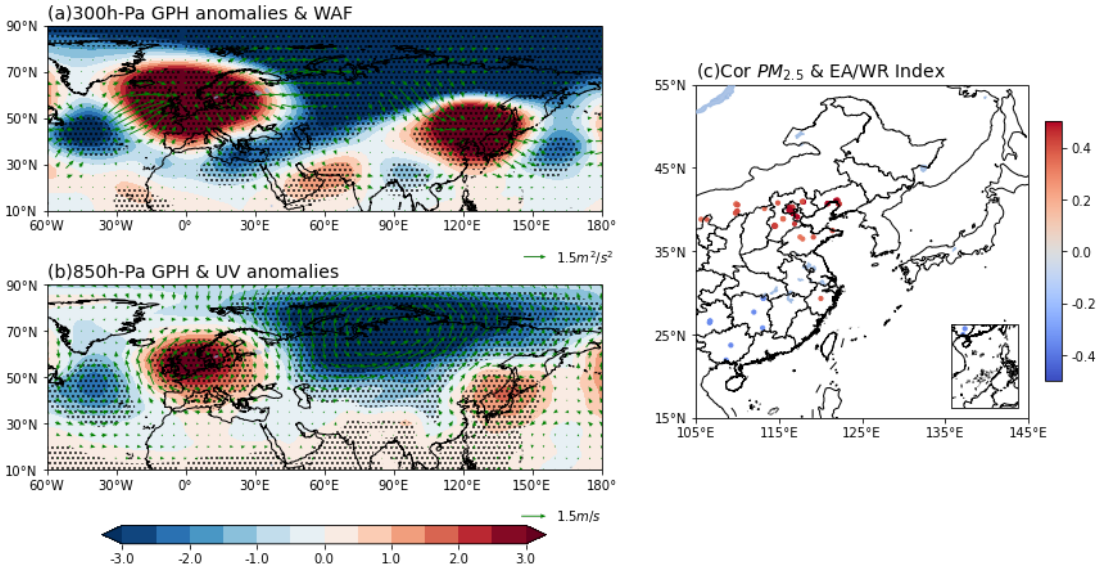

Figure 7. Composite anomalies of (a) GPH (shading; gpm) and WAF (vectors; $m^2\ s^{-2}$) at 300-hPa, and (b) GPH (shading; gpm) and horizontal wind (vectors; $m\ s^{-1}$) at 850-hPa for Type2. Dotted areas are statistically significant at the 95% confidence level. (c) Correlation coefficients between Type2 $PM_{2.5}$ concentration and EA/WR index.

It can be found that the second wave-train reaches EC from Europe along with southern Asia, forming a '+- + - +' pattern of GPH anomalies. The formation of such a wave-train is closely related to the winter East Asia subtropical jet (EASJ) (Xiao et al., 2016; An et al., 2020; Zhang et al., 2022). Here we use an Empirical orthogonal function (EOF) analysis of zonal wind from 1980 to 2021 to determine the leading modes of winter EASJ (Xiao et al., 2016). The variance of the first mode (EOF1) accounts for 57.4% of the total variance and indicates the intensity of EASJ (Figure 8a), which could significantly affect the haze pollution in EC (An et al., 2020; Zhang et al., 2022).

The correlation coefficients between daily $PM_{2.5}$ concentration and the first principle component (PC1_jet) during the occurrence of circulation Type2 is shown in Figure 8b, which has significant positive correlations in south EC and negative correlations in north EC. It indicates that the circulation Type2 may cause severe haze pollution in most areas of EC under the joint affection of EA/WR teleconnection and winter EASJ. The results suggested that when discussing the impact of an anticyclonic anomaly in Northeast Asia on haze pollution in EC, we should comprehensively consider the joint affection of signals from high and middle latitudes.

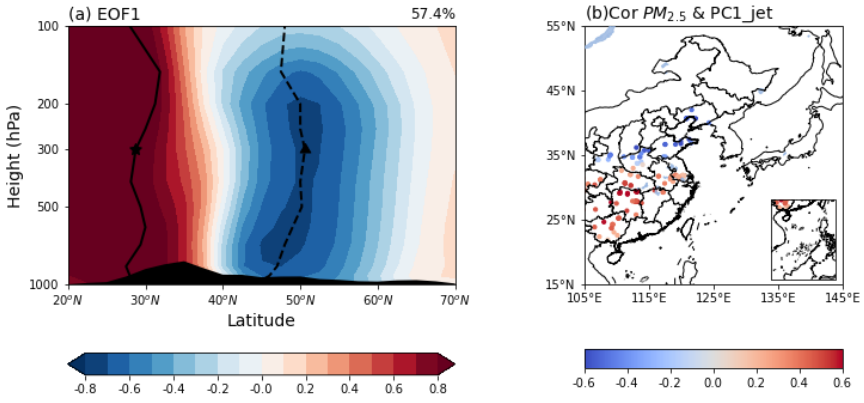

Figure 8. (a) The first EOF mode of zonal wind (EOF1, m s^{-1}) averaged from 60°E to 160°E in NDJF. The star and circular at 300-hPa denote the subtropical jet and polar-front jet cores, respectively. The zonal mean orography is dark-shaded. (b) Correlation coefficients between Type2 $PM_{2.5}$ concentration and PC1_jet.

Compared with circulation Type2, the range and intensity of anticyclonic anomalies in Northeast Asia circulation Type3 are more robust, and the location is more northerly (Figure 9a). Such circulation anomalies lead to southeasterly wind anomalies at 850-hPa, strong TIP, and abundant moisture that induces severe haze over NEC (Figure 9d, f). In addition, the ascending motion over

the south EC and the descending motion over the Beijing–Tianjin–Hebei region and NEC formed meridional circulation cell anomalies (Figure 9e), which are conducive to the accumulation of severe HD_{EC} over the NEC.

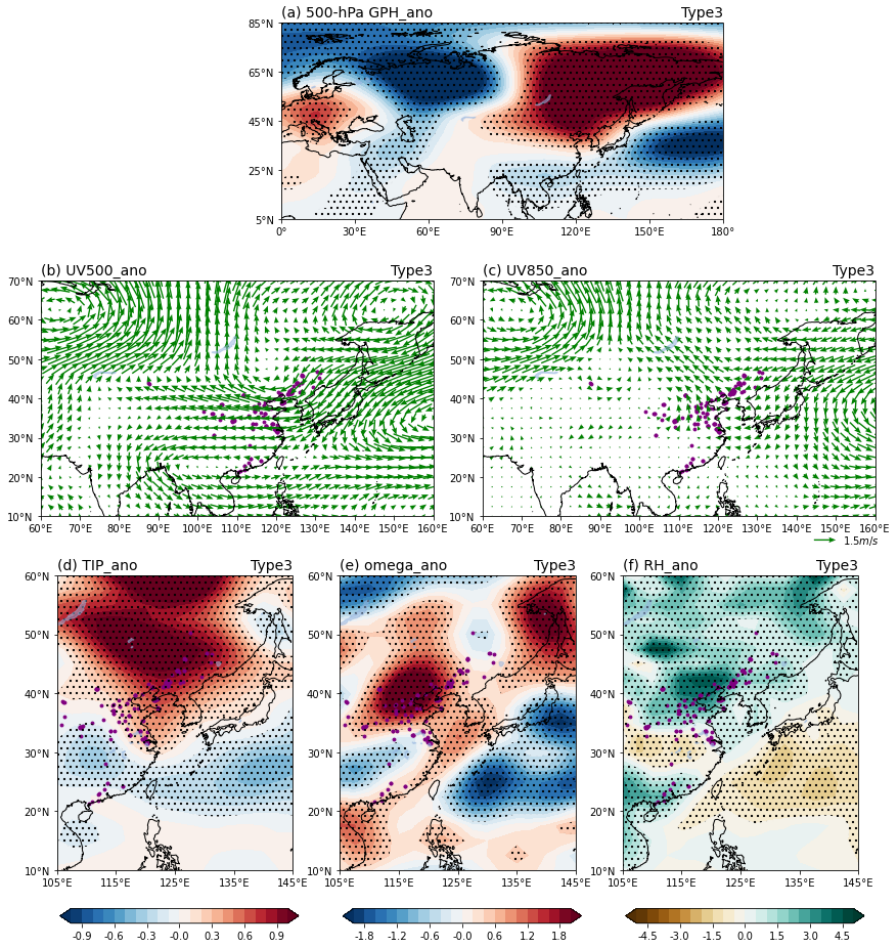

Figure 9. Composite anomalies of (a) GPH at 500-hPa (unit: gpm), horizontal wind (unit: m s^{-1}) at (b) 500-hPa and (c) 850-hPa, (d) TIP (unit: K), (e) omega (unit: 10^{-2} Pa s^{-1}), and (f) RH (unit: %) for circulation Type3. Dotted areas are statistically significant at the 95% confidence level.

In winter, the anticyclonic anomalies over the Okhotsk Sea are usually related to atmospheric blocking (Yun and Yoo 2019; Fang et al., 2020; Hwang et al., 2022). Therefore, we calculated the daily atmospheric blocking introduced in section 2.3 to investigate the relationship between Type3 severe HD_{EC}. Figure 10 shows that when Type3 severe HD_{EC} occurs, the $PM_{2.5}$ concentration increases with the blocking anomalies in the high-latitudes build-up, dissipating with the blocking anomalies crash. The blocking anomalies strengthen the TIP and sufficient RH in the lower atmosphere (Figure 11), causing severe HD_{EC} in NEC.

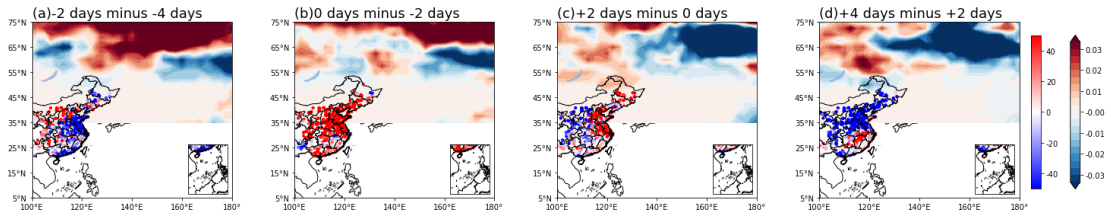

Figure 10. Composite anomalies of (a-d) the spatial distribution of $PM_{2.5}$ concentration variations (unit: μg m^{-3}) and blockings from -4 days to 4 days related to Type3 severe HD_{EC} occur.

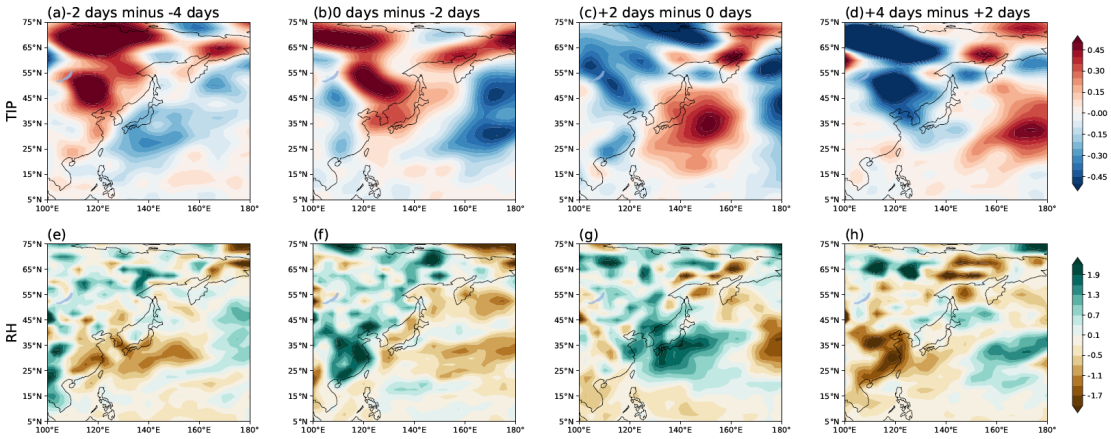

Figure 11. Composite anomalies of (a-d) TIP variations (unit: K) and (e-h) RH variations (unit: %) from -4 days to 4 days related to Type3 severe HD_{EC} occur.

Based on the previous studies and the differences in the influence range of the three circulations types in this study, we divided the EC into NEC (40°N-54°N, 105°E -135°E), North China (NC; 33°N-40°N, 105°E -122°E), the YRV (27°N-33°N, 105°E -122°E), and SC (22°N-27°N, 105°E -122°E) to analyze the temporal characteristics of three HD_{EC} types in different subregions of EC (Figure 12a). Figure 12b, c, d, and e display the annual regional averaged frequency of the three HD_{EC} types in the four subregions. The results show that severe haze pollution mainly occurs in NC and less in SC. The frequency of severe haze generally shows a downward trend in the four subregions.

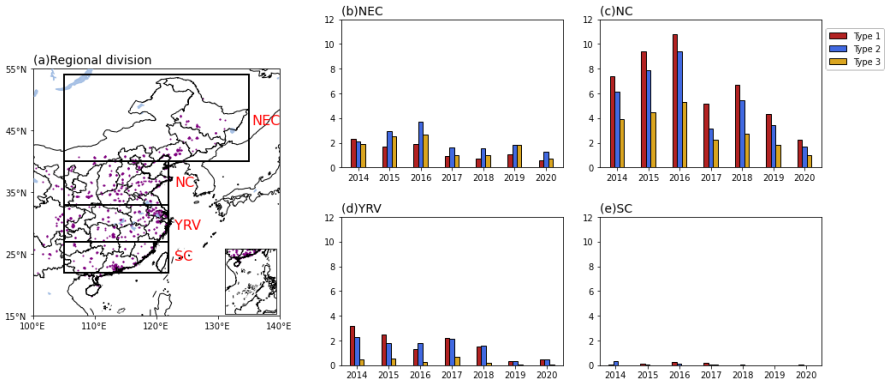

Figure 12. (a) The four subregions of EC. The purple dots are the stations. (b-e) Frequency of three types of cool season severe HD_{EC} in NEC, NC, YRV, and SC.

We further calculated the proportion of the frequency of each circulation type in the total annual severe haze frequency in the four subregions (Figure 13). For NEC, the proportion of the three circulation types is almost equal. It should be noted that the proportion of the circulation Type3 is much larger than that in the other three subregions. In NC, the proportion of the circulation Type1 is more than 40%, while the proportion of the circulation Type3 is about 20%. For YRV, circulation Type1 and Type2 lead the severe haze pollution. There are relatively few severe haze pollution in SC. Therefore, the dominant circulation type in SC has strong interannual variation and is hardly affected by the circulation Type3. Overall, on the weather scale, the HD_{EC} is affected by a variety of synoptic circulations, and the areas affected by each synoptic circulation are also different.

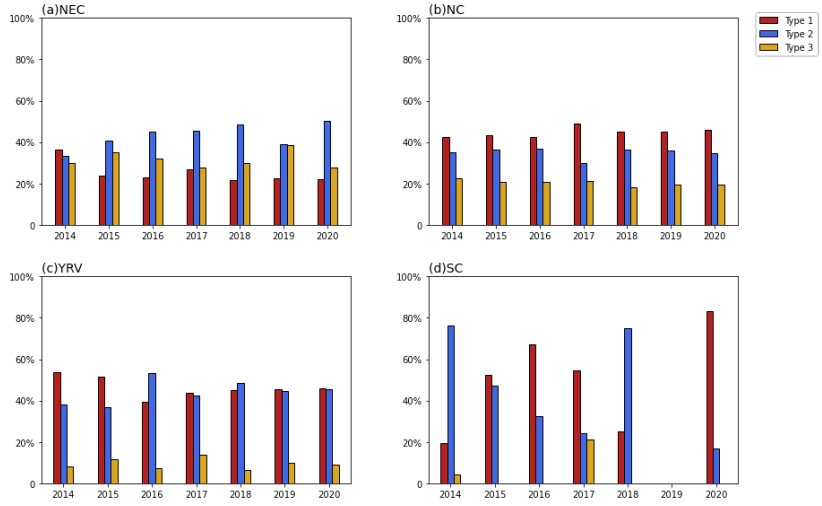

Figure 13. Annual percentage of the three types of severe HD_{EC} in (a) NEC, (b) NC, (c) YRV, and (d) SC.

5. Conclusions and discussion

In this study, the Hierarchical Clustering Algorithm was used to investigate three dominant circulation types that could lead to severe HD_{EC}. We cluster the circulations over the stations in EC on the severe haze days from 2014 to 2021, which eliminates the interference of the circulations of non-severe haze days on the cluster results. The results show that three dominant circulation types associated with severe HD_{EC} are obtained, which are mainly characterized by a local anticyclonic anomaly but also present obvious spatial variation on large scale circulations. The circulation Type1 with wave-train structure of "-+-" in the upper troposphere mainly causes severe haze pollution in the YRV through the low-level north wind anomalies over NC. Although the sinking movement, TIP, and RH anomalies over the YRV are weak or not significant, the regional haze transportation leads to the severe haze in the YRV. The circulation Type2 is characterized by two quasi-barotropic Rossby wave trains at 300-hPa, which may be stimulated and sustained by the joint affection of EA/WR teleconnection and the winter EASJ. One travels from the south of Greenland across Siberia to NEC, forming a '-+-+' pattern of GPH anomalies, and the other travels from Europe along with southern Asia, forming a '+-+-+' pattern of GPH anomalies, which led an anticyclonic over northeastern Asia and conducive to the accumulation of haze. The circulation Type3 is characterized by blocking anomaly over Okhotsk Sea, which influences the severe HD_{EC} over NEC with southeasterly wind at 850-hPa, strong TIP, and abundant moisture. The temporal characteristics of three circulation types in NEC, NC, YRV, and SC were further analyzed. The result shows that on the synoptic scale, HD_{EC} is affected by various synoptic atmospheric circulations, and the regions affected by each synoptic atmospheric circulation are also different.

The study shows that circulation patterns and key systems that contribute to severe HD_{EC} are complex and diverse revealing the dominant circulation patterns of severe haze in different regions of EC. These three dominant atmospheric circulation patterns could be potentially used to establish severe winter haze prediction models for different regions of EC (e.g., project the future variations of severe haze in different regions of EC by identifying similar circulation patterns through machine learning or regression fitting). Due to the limitation of data, it is difficult to carry out the work of circulation classification over a longer period. Therefore, whether there is an interannual or interdecadal connection between the dominant circulation types of severe haze and its key

circulation system needs further investigation. In addition, considering the latitude difference of $PM_{2.5}$ concentrations in EC and the decreasing of $PM_{2.5}$ concentrations due to implementation of the Air Pollution Prevention and Control Action Plan since 2013, the flexible threshold to identify haze day is suggested to use in the further studies. And we will further carefully compare the impact of emissions and meteorological factors on haze in subsequent work.

This study shows that different circulation types may lead to severe haze in different regions of EC, and further studies are needed to investigate whether there are differences in persistence or intensity among them.

Data availability

The Daily $PM_{2.5}$ concentrations for 935 meteorological stations in China are collected by the China National Environmental Monitoring Centre archive at: https://quotsoft.net/air/ (last access: 16 May 2022). Daily mean meteorological data are obtained from the NCEP/NCAR reanalysis data archive at: https://psl.noaa.gov/data/gridded/data.ncep.reanalysis.pressure.html (last access: 16 May 2022, NCEP/NCAR, 2022). The monthly EA/WR Index (CPC, 2022) can be downloaded from NOAA's Climate Prediction Center: http://www.cpc.ncep.noaa.gov/data/teledoc/telecontents.shtml (last access: 16 May 2022).

Competing interests

The authors declare that they have no conflict of interest.

Author contributions

SZ and GZ put forward the conception of this paper, TW improved the research and manuscript. SZ, XY and IV performed research. SZ wrote the manuscript with contributions from all co-authors.

Acknowledgments

This research is supported by the National Natural Science Foundation of China (42175035 and 42077192) and the Postgraduate Research & Practice Innovation Program of Government of Jiangsu Province (KYCX22_1162).

References

An, X., Sheng, L., Liu, Q., Li, C., Gao, Y., Li, J.: The combined effect of two westerly EAJS waveguides on heavy haze in the North China plain in November and December 2015. Atmos. Chem. Phys. 20 (8), 4667–4680. https://doi.org/10.5194/acp-20-4667-2020, 2020.

Barnston, A. G. and Livezey, R. E.: Classification, seasonality and persistence of low frequency atmospheric circulation patterns, Mon. Weather Rev., 115, 1083–1126, 1987.

Cai, W. J., Li, K., Liao, H., Wang, H. J., and Wu, L. X.: Weather Conditions Conducive to Beijing Severe Haze More Frequent under Climate Change, Nat. Clim. Change, 7, 257–262, https://doi.org/10.1038/nclimate3249, 2017.

Cai, W., Xu, X., Cheng, X., Wei, F., Qiu, X., and Zhu, W.: Impact of "blocking" structure in the troposphere on the wintertime persistent heavy air pollution in northern China, Sci. Total Environ., 741, 140325, https://doi.org/10.1016/j.scitotenv.2020.140325, 2020.

Chang, W., & Zhan, J.: The association of weather patterns with haze episodes: Recognition by $PM_{2.5}$ oriented circulation classification applied in Xiamen, Southeastern China, Atmospheric Research, 197, 425 436, http://dx.doi.org/10.1016/j.atmosres.2017.07.024, 2017.

Chen, H. P., Wang, H.J.: Haze Days in North China and the associated atmospheric circulations based on daily visibility data from 1960 to 2012, Journal of Geophysical Research: Atmospheres, 120(12), 5895–5909, https://doi.org/10.1002/2015JD023225, 2015.

Ding, X., Zhang, Y.Q., He, Q.F., Yu, Q.Q., Shen, R.Q., Zhang, Y.L., Zhang, Z., Lyu, S.J., Hu, Q.H., Wang, Y.S., Li, L.F., Song, W., Wang, X.M.: Spatial and seasonal variations of secondary organic aerosol from terpenoids over China. J. Geophys. Res. Atmos, 121, 14661–14678, https://doi.org/10.1002/2016JD025467, 2016.

Ding, Y. H., and Liu, Y. J.: Analysis of long-term variations of fog and haze in China in recent 50

411 years and their relations with atmospheric humidity, Sci. China Ser. D: Earth Sci., 57, 36–46,
412 https://doi.org/10.1007/s11430-013-4792-1, 2014.
413 Fan, X. Q., Sun, Z. B: Analysis on Features of Haze Weather in Xiamen City during 1953–2008.
414 Trans. of Atmos. Sci. 32, 604–609, 2019.
415 Fang, B., & Lu, M.: Heatwave and blocking in the Northeastern Asia: Occurrence, variability, and
416 association, Journal of Geophysical Research: Atmospheres, 125, e2019JD031627.
417 https://doi.org/10.1029/2019JD031627, 2020.
418 Gong, S., Liu, Y., He, J., Zhang, L., Lu, S., & Zhang, X.: Multiscale analysis of the impacts of
419 meteorology and emissions on $PM_{2.5}$ and O_3 trends at various regions in China from 2013 to 2020
420 1: Synoptic circulation patterns and pollution, Science of The Total Environment, 815, 152770,
421 http://dx.doi.org/10.1016/j.scitotenv.2021.152770, 2022.
422 Hu, B., Chen, R., Xu, J. X., Yang, G. S., Xu, D. D., Chen, C. Y., and Zhao, Y . L.: Health effects of
423 ambient ultrafine (nano) particles in haze, Chinese Sci. Bull., 60, 2808–2823,
424 https://doi.org/10.1360/N972014-01404, 2015 (in Chinese).
425 Hwang, J., Son, SW., Martineau, P., Barriopedro, D.: Impact of winter blocking on surface air
426 temperature in East Asia: Ural versus Okhotsk blocking, Climate Dynamics,
427 https://doi.org/10.1007/s00382-022-06204-5, 2022.
428 Kalnay, E., Kanamitsu, M., Kistler, R., Collins,W., Deaven, D., Gandin, L., Iredell,M., Saha, S.,
429 White, G., Woollen, J., Zhu, Y., Leetmaa, A., Reynolds, R., Chelliah, M., Ebisuzaki, W., Higgins,
430 W., Janowiak, J., Mo, K.C., Ropelewski, C., Wang, J., Jenne, R., Joseph, D, The NCEP/NCAR
431 40-year reanalysis project. B. Am. Meteorol. Soc, 77, 437–471, https://doi.org/10.1175/1520-
432 0477(1996)077b0437:TNYRPN2.0.CO;2, 1996.
433 Leung, D. M., Tai, A. P. K., Mickley, L. J., Moch, J. M., van Donkelaar, A., Shen, L., and Martin,
434 R. V.: Synoptic meteorological modes of variability for fine particulate matter ($PM_{2.5}$) air quality
435 in major metropolitan regions of China, Atmos. Chem. Phys., 18, 6733–6748,
436 https://doi.org/10.5194/acp-18-6733-2018, 2018.
437 Li, J., Liao, H., Hu, J., and Li, N.: Severe particulate pollution days in China during 2013–2018 and
438 the associated typical weather patterns in Beijing-Tianjin-Hebei and the Yangtze River Delta
439 regions, Environ. Pollut., 248, 74–81, 2019.

Li, K., Jacob, D. J., Liao, H., Qiu, Y. L., Shen, L., Zhai, S. X., Bates, K. H., Sulprizio, M. P., Song, S. J., Lu, X., Zhang, Q., Zheng, B., Zhang, Y. L., Zhang, J. Q., Lee, H. C., Kuk, S. K.: Ozone pollution in the North China Plain spreading into the late-winter haze season, Proceedings of the National Academy of Sciences, 118(10): e2015797118, https://doi.org/10.1073/pnas.2015797118, 2022.

Li J., X. Hao, H. Liao, Y. Wang, W. Cai, K. Li, X. Yue, Y. Yang, H. Chen, Y. Mao, Y. Fu, L. Chen, and J. Zhu, Winter particulate pollution severity in North China driven by atmospheric teleconnections, Nature Geoscience, 15, 349-355, doi:10.1038/s41561-022-00933-2, 2022.

Li, J., Liao, H., Hu, J., & Li, N.: Severe particulate pollution days in China during 2013 2018 and the associated typical weather patterns in Beijing Tianjin Hebei and the Yangtze River Delta regions, Environmental Pollution, 248, 74 81, https://doi.org/10.1016/j.envpol.2019.01.124, 2019.

Li, Q., Zhang, R. H., and Wang, Y.: Interannual variation of the winter-time fog–haze days across central and eastern China and its relation with East Asian winter monsoon. Int. J. Climatol., 36, 346–354, https://doi.org/10.1002/joc.4350, 2015.

Liao, Z., Xie, J., Fang, X., Wang, Y., Zhang, Y., Xu, X., & Fan, S.: Modulation of synoptic circulation to dry season $PM_{2.5}$ pollution over the Pearl River Delta region: An investigation based on self organizing maps, Atmospheric Environment, 230, 117482, https://doi.org/10.1016/j.atmosenv.2020.117482, 2020.

Liu, N., Zhou, S., Liu, C., & Guo, J.: Synoptic circulation pattern and boundary layer structure associated with $PM_{2.5}$ during wintertime haze pollution episodes in Shanghai, Atmospheric Research, 228, 186 195, https://doi.org/10.1016/j.atmosres.2019.06.001, 2019.

Liu, X., Hui, Y., Yin, Z. Y., Wang, Z., Xie, X., Fang, J.: Deteriorating haze situation and the severe haze episode during December 18–25 of 2013 in Xi'an China, the worst event on record, Theor. Appl. Climatol, https://doi.org/10.1007/s00704-015-1509-8, 2015.

Monks, P., Granier, C., Fuzzi, S., Stohl, A., Williams, M., Akimoto, H., Amann, M., Baklanov, A., Baltensperger, U., Bey, I.: Atmospheric composition change–Global and regional air quality, Atmos. Environ, 43, 5268–5350, https://doi.org/10.1016/j.atmosenv.2009.08.021, 2009.

Niu, F., Li, Z. Q., Li, C., Lee, K. H., Wang, M. Y.: Increase of wintertime fog in China: Potential impacts of weakening of the eastern Asian monsoon circulation and increasing aerosol loading, J.

469 Geophys. Res., 115, D00K20, https://doi.org/10.1029/2009JD013484, 2010.
470 Plumb, R.A.: On the three-dimensional propagation of stationary waves, J. Atmos. Sci, 42, 217–
471 229, https://doi.org/10.1175/1520-0469(1985)042,0217:OTTDPO.2.0.CO;2, 1985.
472 Qian, Y., Gong, D., Fan, J., Leung, L.R., Bennartz, R., Chen, D., Wang, W.: Heavy pollution
473 suppresses light rain in China: Observations and modeling, J. Geophys. Res., 114,
474 https://doi.org/10.1029/2008JD011575, 2009.
475 Rokach, L., Maimon, O.: Clustering methods. Data mining and knowledge discovery handbook,
476 Springer US, 321-352, 2005.
477 Rousseeuw, P.: Silhouettes: A graphical aid to the interpretation and validation of cluster analysis.
478 Journal of Computational and Applied Mathematics, 20, 5365, https://doi.org/10.1016/0377-
479 0427(87)90125-7, 1987.
480 Shen, L., Jacob, D. J., Mickley, L. J., Wang, Y., and Zhang, Q.: Insignificant effect of climate change
481 on winter haze pollution in Beijing, Atmos. Chem. Phys., 18, 17489–17496,
482 https://doi.org/10.5194/acp-18-17489-2018, 2018.
483 Shi, C., Zhang, H., Roth, M., Li, Z.: Impacts of urbanization on long-term fog variation in Anhui
484 Province, China. Atmos. Environ, 42, 8484–8492, https://doi.org/10.1016/j.atmosenv.2008.08.002,
485 2008.
486 Sun, Y., Chen, C., Zhang, Y., Xu, W., Zhou, L., Cheng, X., Zheng, H., Ji, D., Li, J., Tang, X., Fu, P.,
487 Wang, Z.: Rapid formation and evolution of an extreme haze episode in Northern China during
488 winter 2015, Sci. Rep. 6, 27151, https://doi.org/10.1038/srep27151, 2016.
489 Sun, Y., Ma, Z. F., Niu, T.R., Fu, Y., Hu, J.F.: Characteristics of climate change with respect to fog
490 days and haze days in China in the past 40 years. Clim. Environ. Res.,18, 397–406, 2013.
491 Sun, Y., Niu, T., He, J., Ma, Z., Liu, P., Xiao, D., ... & Yan, X.: Classification of circulation patterns
492 during the formation and dissipation of continuous pollution weather over the Sichuan Basin,
493 China, Atmospheric Environment, 223, 117244, https://doi.org/10.1016/j.atmosenv.2019.117244,
494 2020.
495 Tibaldi, S., and F. Molteni: On the operational predictability of blocking. Tellus, 42A,343–365, 1990.
496 Tsaia, F., Tu, J. Y., Hsu, S. C., Chen, W. N.: Case study of the Asian dust and pollutant event in
497 spring 2006: Source, transport, and contribution to Taiwan, Sci. Total Environ, 478, 163–174,

https://doi.org/10.1016/j.scitotenv.2014.01.072, 2014.

Wang, H. J., Chen, H. P., Liu, J. P.: Arctic Sea Ice Decline Intensified Haze Pollution in Eastern China. Atmos. Oceanic Sci., 8:1, 1-9, https://doi.org/10.3878/AOSL20140081, 2015.

Wang, K. C., Dickinson, R. E., Liang, S. L.: Clear sky visibility has decreased over land globally from 1973 to 2007, Science, 323, 1468–1470, https://doi.org/10.1126/science.1167549, 2009.

Wang, X. Y., Zhang, R. H., Tan, Y. K., Yu, W.: Dominant synoptic patterns associated with the decay process of $PM_{2.5}$ pollution episodes around Beijing, Atmos. Chem. Phys., 21, 2491–2508, https://doi.org/10.5194/acp-21-2491-2021, 2021.

Wang, X.Y., Dickinson, R.E., Su, L.Y., Zhou, C.L., Wang, K.C.: $PM_{2.5}$ pollution in China and how it has been exacerbated by terrain and meteorological conditions, Bulletin of the American Meteorological Society, 99(1): 105-119, https://doi.org/10.1175/BAMS-D-16-0301.1, 2018.

Wang, X.Y., Zhang, R.H., Effects of atmospheric circulations on the interannual variation in $PM_{2.5}$ concentrations over the Beijing–Tianjin–Hebei region in 2013–2018, 20, 7667-7682, https://doi.org/10.5194/acp-20-7667-2020, 2020.

Wang, Z.S., Liu, X.D., Xie, X.N.: Effects of Strong East Asian Cold Surges on Improving the Air Quality over Mainland China, Atmosphere, 7, 38, https://doi.org/10.3390/atmos7030038, 2016.

Wei, Y., Li, J., Wang, Z., Chem, H., Wu, Q., Li, J., Wang, Y., and Wang, W.: Trends of surface $PM_{2.5}$ over Beijing–Tianjin–Hebei in 2013–2015 and their causes: emission controls vs. meteorological conditions, Atmos. Oceanic Sci. Lett., 10, 276–283, https://doi.org/10.1080/16742834.2017.1315631, 2017.

Wu, M., Wu, D., Fan, Q., Wang, B. M., Li, H. W., Fan, S. J.: Observational studies of the meteorological characteristics associated with poor air quality over the Pearl River Delta in China, Atmos. Chem. Phys, 13, 10755–10766, https://doi.org/10.5194/acp-13-10755-2013, 2013.

Wu, P., Ding, Y. H., Liu, Y. J., and Li, X. C.: Influence of the East Asian winter monsoon and atmospheric humidity on the wintertime haze frequency over central-eastern China, Acta Meteorol. Sin., 74, 352–366, https://doi.org/10.11676/qxxb2016.029, 2016 (in Chinese).

Wu, P., Ding, Y., and Liu, Y.: Atmospheric circulation and dynamic mechanism for persistent haze events in the Beijing–Tianjin–Hebei region, Adv. Atmos. Sci., 34, 429–440, 2017.

Xiao, C., Zhang, Y., Lofgren, B. M., & Nie, Y.: The concurrent variability of East Asian subtropical

527 and polar-front EAJSs and its implication for the winter climate anomaly in China, Journal of
528 Geophysical Research: Atmospheres, 121(12), 6787-6801, 2016.
529 Xie, Y. B., Chen, J., and Li, W.: An assessment of PM2:5 related health risks and impaired values
530 of Beijing residents in a consecutive high-level exposure during heavy haze days, Environ. Sci.,
531 35, 1–8, 2014.
532 Xu, J., Yan, F., Xie, Y., Wang, F., Wu, J., Fu, Q.: Impact of meteorological conditions on a nine-day
533 particulate matter pollution event observed in December 2013, Shanghai, China, Particuology, 20,
534 69–79, https://doi.org/10.1016/j.partic.2014.09.001, 2015.
535 Yang, Y., Zhou, Y., Li, K., Wang, H., Ren, L., Zeng, L., ... & Liao, H.: Atmospheric circulation
536 patterns conducive to severe haze in eastern China have shifted under climate change, Geophysical
537 Research Letters, 48(23), e2021GL095011, https://doi.org/10.1029/2021GL095011, 2021.
538 Yin, Z. C. and Wang, H. J.: The relationship between the subtropical Western Pacific SST and haze
539 over North-Central North China Plain, Int. J. Climatol., 36, 3479–3491,
540 https://doi.org/10.1002/joc.4570, 2016.
541 Yin, Z. C., Wang, H. J., and Chen, H. P.: Understanding severe winter haze events in the North
542 China Plain in 2014: roles of climate anomalies, Atmos. Chem. Phys., 17, 1641–1651,
543 https://doi.org/10.5194/acp-17-1641-2017, 2017.
544 Yin, Z. C., Wang, H. J., and Yuan, D. M.: Interdecadal increase of haze in winter over North China
545 and the Huang-huai area and the weakening of the East Asia winter monsoon. Chin. Sci. Bull., 60,
546 1395–1400, 2015
547 Yin, Z. C., Wang, H. J.: Possible Relationship between the Chukchi Sea Ice in the Winter and the
548 February Haze Pollution in the North China Plain, Journal of Climate, 32(16), 5179-5190,
549 https://doi.org/10.1175/JCLI-D-18-0634.1, 2019.
550 Yin, Z. C., Wang, H. J.: Role of atmospheric circulations in haze pollution in December 2016,
551 Atmospheric Chemistry and Physics, 17(18): 11673-11681, https://doi.org/10.5194/acp-17-11673-
552 2017, 2017.
553 Yin, Z. C., Zhang, Y.J., Wang, H.J., Li, Y.Y., Evident $PM_{2.5}$ drops in the east of China due to the
554 COVID-19 quarantine measures in February, Atmospheric Chemistry and Physics, 21, 1581-1592,
555 https://doi.org/10.5194/acp-21-1581-2021, 2021.

Yun, S., Yoo, C.: The effects of spring and winter blocking on PM10 Concentration in Kore, Atmosphere, 10(7): 410, https://doi.org/10.3390/atmos10070410, 2019.

Zhang, S.Y., Zeng, G., Yang, X.Y., Wu, R.X., Yin, Z.C.: Comparison of influence between two types of cold surge on haze dispersion in Eastern China, Atmospheric Chemistry and Physics, 21, 15185-15197, https://doi.org/10.5194/acp-21-15185-2021, 2021.

Zhang, S.Y., Zeng, G., Wang, T.J., Yang, X.Y., Vedaste, I.: Interannual relationship between displacement and intensity of East Asian jet stream and haze over eastern China in winter, Science of the Total Environment, http://dx.doi.org/10.1016/j.scitotenv.2022.154672, 2022.

Zhong, W. G., Yin, Z. C., Wang, H. J.: The relationship between anticyclonic anomalies in northeastern Asia and severe haze in the Beijing–Tianjin–Hebei region, Atmos. Chem. Phys., 19, 5941-5957, https://doi.org/10.5194/acp-19-5941-2019, 2019.